Please cite this article in press as: Golbek et al., Otoferlin C2F Domain-Induced Changes in Membrane Structure Observed by Sum Frequency Generation, Biophysical Journal (2019), https://doi.org/10.1016/j.bpj.2019.09.010

Biophysical *Journal*
Article

Biophysical Society

Otoferlin C2F Domain-Induced Changes in Membrane Structure Observed by Sum Frequency Generation

Thaddeus W. Golbek,[1,3] Murugesh Padmanarayana,[2] Steven J. Roeters,[3] Tobias Weidner,[3] Colin P. Johnson,[2,*] and Joe E. Baio[1,*]

[1]School of Chemical, Biological, and Environmental Engineering and [2]Department of Biochemistry and Biophysics, Oregon State University, Corvallis, Oregon; and [3]Department of Chemistry, Aarhus University, Aarhus, Denmark

ABSTRACT Proteins that contain C2 domains are involved in a variety of biological processes, including encoding of sound, cell signaling, and cell membrane repair. Of particular importance is the interface activity of the C-terminal C2F domain of otoferlin due to the pathological mutations known to significantly disrupt the protein's lipid membrane interface binding activity, resulting in hearing loss. Therefore, there is a critical need to define the geometry and positions of functionally important sites and structures at the otoferlin-lipid membrane interface. Here, we describe the first in situ probe of the protein orientation of otoferlin's C2F domain interacting with a cell membrane surface. To identify this protein's orientation at the lipid interface, we applied sum frequency generation (SFG) vibrational spectroscopy and coupled it with simulated SFG spectra to observe and quantify the otoferlin C2F domain interacting with model lipid membranes. A model cell membrane was built with equal amounts of phosphatidylserine and phosphatidylcholine. SFG measurements of the lipids that make up the model membrane indicate a 62% increase in amplitude from the SFG signal near 2075 cm^{-1} upon protein interaction, suggesting domain-induced changes in the orientation of the lipids and possible membrane curvature. This increase is related to lipid ordering caused by the docking interaction of the otoferlin C2F domain. SFG spectra taken from the amide-I region contain features near 1630 and 1670 cm^{-1} related to the C2F domains beta-sandwich secondary structure, thus indicating that the domain binds in a specific orientation. By mapping the simulated SFG spectra to the experimentally collected SFG spectra, we found the C2F domain of otoferlin orients 22° normal to the lipid surface. This information allows us to map what portion of the domain directly interacts with the lipid membrane.

SIGNIFICANCE The encoding of sound within the ear is carried out by specific protein-lipid membrane interactions. In healthy sensory cells, the protein otoferlin has been identified as the regulator of this process. Mutations within otoferlin disrupt the protein's lipid membrane binding activity, resulting in hearing loss. In this investigation, we apply a label-free spectroscopy method coupled with theoretical modeling to characterize the specific interactions between otoferlin and a lipid membrane in situ. The advancement of this label-free spectroscopy method has allowed us to overcome the limitations of current structural biology-based techniques. Therefore, shedding light on in situ interactions of biologically relevant membrane proteins and cellular membranes.

INTRODUCTION

Protein function is dependent on both its structure and how the protein binds to other materials. This is especially true for protein-protein docking, proteins that interact and self-assemble in soft tissues, proteins that recognize specific mineral facets, proteins that are a part of functional biomaterials, and proteins that are cell membrane receptors (1). Within this conceptual framework, the encoding of sound within the ear is carried out by specific protein-lipid membrane interactions. In healthy sensory cells, the protein otoferlin has been identified as the regulator of this process (2,3). Mutations within otoferlin are known to significantly disrupt the protein's lipid membrane binding activity, resulting in auditory neuropathy and nonsyndromatic hearing loss (4,5). The specific protein-membrane interactions that contributes to the sound encoding process appear to be fundamentally grounded in precise chemical processes.

Submitted February 26, 2019, and accepted for publication September 10, 2019.

*Correspondence: colin.johnson@oregonstate.edu or joe.baio@oregonstate.edu

Editor: Arne Gericke.

https://doi.org/10.1016/j.bpj.2019.09.010

Please cite this article in press as: Golbek et al., Otoferlin C2F Domain-Induced Changes in Membrane Structure Observed by Sum Frequency Generation, Biophysical Journal (2019), https://doi.org/10.1016/j.bpj.2019.09.010

Therefore, there is a critical need to define the geometry and positions of functionally important sites at the otoferlin-lipid membrane interface. Insights into binding interactions can lead to an accurate dissection of vital chemical interactions that control sound signaling pathways. Without this structural information, treating diseases linked to this form of hearing loss will likely remain challenging. Therefore, in this investigation, we report the use of sum frequency generation (SFG) vibrational spectroscopy, a label-free method, to identify the interaction of a C2 domain of the exocytotic protein otoferlin with a lipid membrane.

Found in sensory hair cells, otoferlin is a 240 kDa protein with six C2 domains that couples, in response to intracellular calcium, to a membrane during exocytosis (6). Typically composed of a β-sandwich fold, the C2 domain represents one of the largest families of membrane binding motifs and is found in numerous protein families, including synaptotagmins, protein kinases, DOC2, and ferlins (6,7). Mechanistically, it is believed that C2 domains target the protein to a particular subcellular location based upon membrane lipid composition, with the loops at one edge of the domain making electrostatic and hydrophobic interactions with the lipid headgroup (8). Additionally, hydrophobic residues within the loops of some C2 domains insert into the bilayer, causing a change of the spontaneous curvature of the membrane, which may facilitate membrane fusion and exocytosis (9,10). A small orientation angle should allow the binding loops to insert into the lipid membrane, whereas a large orientation angle will prevent the docking of this domain. The docking angle between the domain and membrane is thought to be a critical parameter that may throttle protein activity; however, this has not been experimentally determined for the C2F domain of otoferlin. Thus, it is important to determine the binding angle of the C2F domain of otoferlin.

The C2F domain, located on the C-terminus of the otoferlin protein, has garnered considerable interest because of deafness-causing mutations, mapped to this domain (6). Liposome co-sedimentation and noncanonical amino acid studies have established that this domain binds anionic lipids including phosphatidylserine via loops at one end of the domain, which contact the bilayer (11). Like other studies on membrane binding domains, these previous measurements on the C2F domain have relied on the addition of bulky labels through site-directed mutagenesis of the loops that are thought to interact with the membrane, which can alter the binding affinity, specificity, and depth of insertion (12). As a result, the C2 domain-lipid membrane interface represents an important yet understudied area of biological chemistry. Characterization of this interface has been a major challenge because of the considerable difficulties in applying traditional structural biology-based techniques to probe protein structure at lipid surfaces. For example, x-ray powder diffraction or solid-state NMR efforts on protein-lipid samples have had relatively limited success, including the inability to fully capture all protein-lipid interactions (13). Thus, there is a need for a method that provides an accurate characterization of the protein-lipid interface structure without chemical perturbation by labels.

Recently, nonlinear surface spectroscopy techniques including SFG have emerged as a methodology for directly probing protein-membrane interactions in a label-free manner (14–17). SFG is a second order nonlinear optical technique, involving a visible beam that is pulsed in temporal and spatial synchronicity with an infrared laser. The technique is capable of detecting biomolecule adsorption and orientation in submicromolar concentrations at physiological pH (18–23). A particular characteristic of SFG is that spectral contributions of individual protein folding motifs and orientations will interfere in specific ways and therefore can be expected to result in complex vibrational spectra. The challenge is then to disentangle the resulting spectral information. Therefore, specific methods to delineate protein-lipid binding geometries from complex spectra have been previously developed by combining experimental SFG spectra with theoretical SFG spectra calculated from the results of molecular dynamics simulations (1,24–28). Our results provide the first orientation view of any C2 domain of otoferlin docked at a lipid membrane.

MATERIALS AND METHODS

Materials

1,2-dipalmitoyl-*sn*-glycero-3-phospho-L-serine (sodium salt) (DPPS) and 1,2-dipalmitoyl-*sn*-glycero-3-phosphocholine (DPPC) were purchased from Avanti Polar Lipids (Alabaster, AL). Glutathione Sepharose beads were purchased from GE-Amersham Biosciences (Pittsburgh, PA). Other common reagents were obtained from Sigma-Aldrich (St. Louis, MO).

Protein construct and purification

The C2F domain of otoferlin was cloned as a GST-fusion construct into pGEX-6P3 vector. The subcloned C2F domain was verified by DNA sequencing, and the amino acid sequence can be found in the Supporting Materials and Methods. The pGEX-6P3 vector containing the C2F domain was transformed into BL21 *Escherichia coli* cells. The bacterial culture ($OD_{600} = 0.6$) was induced for 12 h at 18°C with 1 mM isopropyl-β-D-thiogalactoside. Cells were pelleted at 4000 rpm and resuspended in lysis buffer containing 40 mM HEPES (pH = 7.5), 200 mM NaCl, and 1 mM dithiothreitol (DTT). The cells were lysed by sonication in lysis buffer containing protease inhibitors (1 mM phenylmethylsulfonyl fluoride and 1–2 μg/mL aprotinin, leupeptin, and pepstatin A). The soluble fraction of lysate was incubated with glutathione resin for 2 h at 4°C, and the resin was washed with lysis buffer before the bound protein was eluted with elution buffer containing HEPES (pH = 7.5) and 200 mM NaCl and 200 mM reduced glutathione. Purified protein was extensively dialyzed in buffer containing 40 mM HEPES (pH 7.5), 200 mM NaCl, 1 mM DTT, and concentrated using an Ultrafree-10 centrifugal filter unit (Pall Corporation, Port Washington, NY). The protein was cleaved from the GST tag with precision protease enzyme overnight at 4°C, and the cut GST tag was removed by incubating with Glutathione Sepharose resin. The pure C2F domain concentration was determined by ultraviolet absorbance at 280 nm.

Please cite this article in press as: Golbek et al., Otoferlin C2F Domain-Induced Changes in Membrane Structure Observed by Sum Frequency Generation, Biophysical Journal (2019), https://doi.org/10.1016/j.bpj.2019.09.010

Phospholipid vesicles

The preparation of SUVs was performed according to reported methods. Powders of DPPS and DPPC were dissolved in chloroform, methanol, and water at the ratio (65:35:8) and in chloroform, respectively. 50% DPPC and 50% DPPS were mixed and dried under a stream of liquid nitrogen and then dried under vacuum overnight. The dried lipids were resuspended in buffer containing HEPES (pH 7.5), 200 mM NaCl, and 1 mM DTT and extruded 20 times through 50-nm filter (Avanti Polar Lipids) to produce small unilamellar vesicles (SUVs). This 1:1 DPPC and DPPS ratio was informed by previous work that demonstrates that otoferlin binds to SUVs composed of 50% DPPS and that the amount of protein bound to the SUVs that did not change the percentage of DPPS was increased from 25 to 50% (29). It has been speculated that the otoferlin C2F domain clusters negatively charged lipids around it, creating a raft of very high density of negative charges.

Flotation assays

Flotation assays using extruded liposomes were performed using procedures described previously (4). Briefly, C2F-liposome assays were performed in either 0.1 mM EGTA or 1 mM free calcium in 20 mM HEPES and 150 mM NaCl (pH 7.5). 15 μM of protein was added to liposome samples before mixing with an Accudenz density medium. The sample was subsequently overlaid with decreasing amounts of Accudenz, forming a step gradient. After centrifugation, the floated liposomes were collected from the Accudenz-buffer interface, resolved by sodium dodecyl sulfate polyacrylamide gel electrophoresis. Stained Coomassie blue gels were imaged and processed using Illustrator (Adobe).

Lipid bilayer setup

A flow cell made from Teflon was used for all experiments. A lipid bilayer prepared from a 50:50 molar ratio of phospholipids DPPC (Avanti Polar Lipids) and DPPS (Avanti Polar Lipids) was deposited on equilateral CaF_2 prisms (Greyhawk Optics, Waltham, MA). DPPS/DPPC vesicles were prepared by rapid solvent exchange by first dissolving the lipids in chloroform, vacuum drying for 1.5 h, and then finally adding D_2O (Carl Roth, Karlsruhe, Germany) for a final concentration of 1 mg/mL. The vesicles were allowed to fuse, forming a bilayer for 2 h before phosphate-buffered saline (0.01 M phosphate buffer, 0.0027 M KCl, and 0.137 M NaCl (pH 7.4); Sigma-Aldrich) made with D_2O and 25 μM $CaCl_2$ was flowed in to wash away the remaining vesicles. Otoferlin C2F domain was flowed in 0.5 mg/mL and allowed to interact for 1 h. Negatively charged lipid bilayers containing DPPS and DPPC are commonly formed with little defects by vesicle fusion at solid substrate interfaces (24,30,31).

Lipid monolayer setup

A lipid monolayer was assembled at the air-water interface within a Teflon trough with a volume of ~10 mL of buffer (40 mM HEPES, 1 mM DTT, 50 mM NaCl, and 200 μM $CaCl_2$) prepared with MilliQ water (Direct-Q3 System; MilliporeSigma, Burlington, MA). The phospholipid 1,2-dipalmitoyl-d62-*sn*-glycero-3-(phospho-L-serine)(sodium salt) (dDPPS) (Avanti Polar Lipids) was first dissolved in a 65:35:8 ratio of chloroform (HPLC grade; J. T. Baker), methanol (ACS grade; Fisher Chemical, Waltham, MA), and MilliQ water, respectively, and 1,2-dipalmitoyl-d62-*sn*-glycero-3-phosphocholine (dDPPC) (Avanti Polar Lipids) was dissolved in chloroform. The lipids were then mixed to yield a 1:1 ratio of dDPPS and dDPPS lipids and then spread by dropwise addition to the aqueous surface via a Hamilton microsyringe until a mean molecular area was reached that corresponded to a liquid-condensed (LC) phase, which was monitored by a tensiometer (KSV NIMA with a Wilhelmy plate) (14,32). A pure dDPPC lipid monolayer was also built as a control. After the assembly of the lipid interface, an otoferlin C2F domain solution was injected into the trough subphase to reach a final concentration of 0.045 mg/mL or 1.6 μM and allowed to interact for 2.5 h.

SFG spectra calculations

The spectral calculations are based on the formalism published in (33) and are described in more detail in the Supporting Materials and Methods. In short, we construct a one-exciton amide-I Hamiltonian for the backbone amide groups in the protein, with a single local-mode frequency (i.e., assuming that, on average, all amide groups are hydrogen bonded equally) and couplings that are modeled differently for nearest- and non-nearest-neighbor amide groups. The nearest-neighbor interactions, dominated by through-bond effects, are modeled using a parameterized map of an ab initio calculation with the 6-31G+(d) basis set and the B3LYP functional, which gives the coupling as a function of the dihedral angle (34,35). The non-nearest-neighbor interactions, dominated by through-space effects, are modeled using the transition-dipole coupling model (36). The Hamiltonian is then diagonalized to obtain the system's eigenvalues and eigenvectors, from which the spectroscopic response is calculated. Because the *ssp* spectrum is dominated by side-chain peaks, it was necessary to explicitly include these peaks as they—through constructive and destructive interference—influence the spectral shape in the amide-I region (1600–1700 cm^{-1}). We thus included three Lorentzian peaks next to the amide-I peak, one centered at 1450 cm^{-1} for the $\delta_{as}(CH_3)$ and $\delta(CH_2)$ vibrations, one centered at 1584 cm^{-1} for the Asp and Glu side chains (37), and one at 1708 cm^{-1} for the C=O groups that are present in the lipid headgroups (15,33). To account for the azimuthal isotropy of the protein at the interface, we average the protein's Euler angle ϕ from 0 to 2π (except in the calculation presented in Fig. S3). We performed a grid search over the other two Euler angles, θ and ψ, to find the minimum in the error-weighted residual sum of squares (RSS) of the total difference between the calculated and experimental spectra in the *ppp* and *ssp* polarization combination (using a single, overall scaling factor to calculate the amide-I response of both polarization combinations). We then performed a free fit in θ and ψ near the RSS minimum to obtain the optimal angles (see Results). The errors on the fit parameters and the correlation matrix of this fit (plotted in Fig. 4 *A*) can be found in Table S2. We model the local-field corrections (Fresnel factors) as described in (20), for which we have assumed the refractive index of CaF_2 for the layer above the interface, using the dispersion relation reported in (38) (leading to $n_{1,SF} = 1.43$, $n_{1,VIS} = 1.43$, and $n_{1,IR} = 1.38$ at the employed frequencies of ~705, 798, and 6100 nm for the SF, VIS, and IR fields, respectively), the refractive index typical for bulk protein solutions (39) for the interfacial refractive indices (leading to $n_i = 1.47$ at all frequencies, because the dispersion is almost negligible for proteins (40)), and the refractive index of bulk H_2O (41) for the layer below the surface (leading to $n_{2,SF} = 1.33$, $n_{2,VIS} = 1.33$, and $n_{2,IR} = 1.32$). An optimal match between calculations and experiment was found for a central frequency (the gas phase frequency minus an overall frequency shift due to hydrogen bonding) of 1651 cm^{-1}, which is in line with previous calculations using the same method (25,42,43), and a Lorentzian width of 15 cm^{-1}, which is in line with the experimentally determined line width of the IR beam. Although (3) contributions based on electrostatic fields can affect the line shape of SFG spectra (44), we have not performed a correction here because no significant electrostatic fields are expected at lipid bilayer surfaces.

Broadband SFG vibrational spectroscopy

A femtosecond Ti: Sapphire laser oscillator coupled with a Nd:YLF laser pumped regenerative amplifier (Spitfire Ace; Spectra-Physics, Santa Clara, CA) was used to generate a visible beam (35 fs pulse duration and 4.65 mJ) centered at 791.8 nm. The amplified visible beam was split into two parts. The first was used as the visible pulse for SFG and was passed through a Fabry-Perot etalon to spectrally narrow the pulse to ~15 cm^{-1}. The second

Please cite this article in press as: Golbek et al., Otoferlin C2F Domain-Induced Changes in Membrane Structure Observed by Sum Frequency Generation, Biophysical Journal (2019), https://doi.org/10.1016/j.bpj.2019.09.010

part was used to pump the optical parametric amplifier system (Light Conversion, TOPAS). The generated tunable infrared pulse (3.1–6.1 μm) was polarized by a half-wave plate before use as the SFG IR pulse. The IR and visible pulses were overlapped temporally and spatially at the liquid-air interface generating an SFG signal. SFG spectra of the samples were collected in the polarization combinations *ppp*, *ssp,* and *s*-polarized SFG, *p*-polarized visible, and *p*-polarized IR (*spp*) amide-I region (1500–1800 cm^{-1}). The resulting SFG signal was focused onto a spectrograph (Action; Teledyne Princeton Instruments, Martinsried, Germany), dispersed by grating, and refocused on an electron multiplying charge coupled device camera (Newton; Andor Technology, Belfast, U.K.). SFG spectra were normalized by division of a clean gold reference. The SFG spectrum were fit with the following equation (45,46):

$$\chi^{(2)}_{eff}(\omega) = \chi^{(2)}_{NR} + \sum_q \frac{A_q}{\omega - \omega_q + i\Gamma_q}, \quad (1)$$

where Γ_q, A_q, and ω_q are the full width half maximal (FWHM), amplitude, and resonant frequency of the q^{th} vibrational mode, respectively, and $\chi^{(2)}_{NR}$ and $\chi^{(2)}_{eff}$ are the nonresonant background and effective seconded nonlinear susceptibility tensor, respectively.

Narrow band SFG vibrational spectroscopy

An EKSPLA Nd:YAG laser, operating at 50 Hz, was used to generate both a fixed visible (532 nm^{-1}) and tunable IR beam (1000–4000 cm^{-1}) via sequential pumping through an EKSPLA optical parametric generation/amplification and difference frequency unit, which utilized barium borate and $AgGaS_2$ crystals, respectively. The bandwidth was 2 cm^{-1} for the visible pump pulses and 4 cm^{-1} for the IR laser. The visible (~150 μJ/pulse) and IR beams (~200 μJ/pulse) were overlapped spatially and temporally at the desired interface at an incident angle of 60 and 54° versus the surface normal to generate SFG photons, which were spectrally filtered, dispersed by a monochromator, and detected with a gated photomultiplier tube. SFG spectra of the samples were collected in the polarization combination *s*-polarized SFG, *s*-polarized visible, *p*-polarized IR (*ssp*) in the CD region (2000–2300 cm^{-1}). Both beams were focused to a ~1-mm diameter at the interface. Spectra were collected in 4 cm^{-1} steps with 400 acquisitions per step. The SFG spectra were normalized by the product of the IR and visible pump beam intensities. The spectra were fit with Eq. 1.

RESULTS AND DISCUSSION

The C2F domain of otoferlin binds liposomes made up of DPPS and DPPC

To confirm that the domain will bind to the lipids in our system, we conducted co-floatation assays. We found that in the in vitro co-floatation assays, the C2F domain of otoferlin bound to DPPS/DPPC but not DPPC liposomes regardless of calcium (Fig. 1, *A* and *B*). Our binding assay results are comparable to previous studies that report that the individual C2F domain binds negatively charged membranes in a calcium-independent manner (11).

The C2F domain of otoferlin changes the lipid curvature

To identify how the protein influences the structure of the lipid layer it is interacting with, SFG spectra were collected at a lipid monolayer surface both before and after the C2F

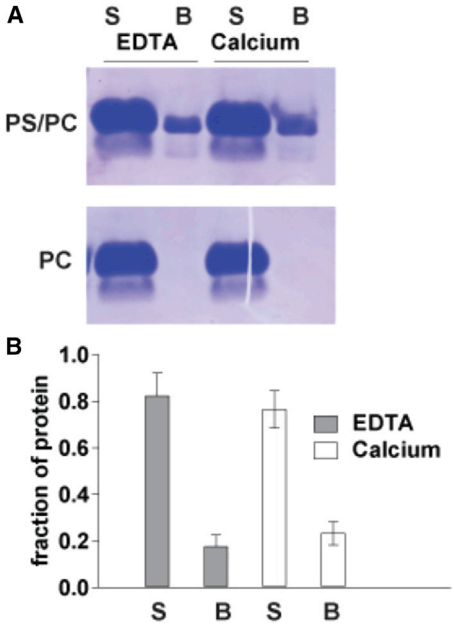

FIGURE 1 (*A*) Representative image of a co-floatation assay with the C2F domain of otoferlin mixed with DPPS/DPPC (1:3) or DPPC SUV in the presence of calcium or EDTA. (*B*) Quantification of the results of the liposome binding assay is shown. S denotes supernatant, and B denotes protein bound to floated liposomes. To see this figure in color, go online.

domain was allowed to interact for 2.5 h. Lipid monolayers provide a simple biomimetic approach to study the structure and interaction of proteins at the lipid membrane interface (14,15,24,32,47–53). Again, as in previous studies, isotopically labeled acyl chain versions of the lipids isolate the vibrations of just the lipid monolayers acyl chains for that of the proteins vibrational CH groups (14,15). SFG spectra for C2F domain of otoferlin interacting with monolayer interfaces in the CD region (2000–2300 cm^{-1}) can be found in Fig. 2, *A–D*, and SFG fitting parameters are found in Table 1. Before the injection of the C2F domain into the subphase, spectra collected contain resonances near 2075, 2125, and 2225 cm^{-1} assigned to the CD_3 symmetric, CD_3 Fermi, and CD_3 asymmetric vibration, respectively (14). In each experiment, the membrane was constructed with a starting surface pressure between 18 and 20 mN/m, at which the DPPC monolayer is in the LC phase (32). After injection and incubation of the protein, the pressure rose to 24 mN/m but the monolayer remained in the LC phase. At this LC phase, we expect that the CD_2 symmetric and CD_2 asymmetric resonances from the lipids near 2100 and 2200 cm^{-1} shall be very weak. In the LC phase, the CD_2 symmetric and CD_2 asymmetric vibrational modes are in an all-*trans* conformation resulting in a low intensity of the vibrational modes seen in the SFG spectrum (14,32,54). Thus, because we are already starting in the LC phase and not the liquid expanded phase, at the start of the experiment, we were not able to fit very small peaks for the CD_2 symmetric and CD_2 asymmetric (54). It should

Please cite this article in press as: Golbek et al., Otoferlin C2F Domain-Induced Changes in Membrane Structure Observed by Sum Frequency Generation, Biophysical Journal (2019), https://doi.org/10.1016/j.bpj.2019.09.010

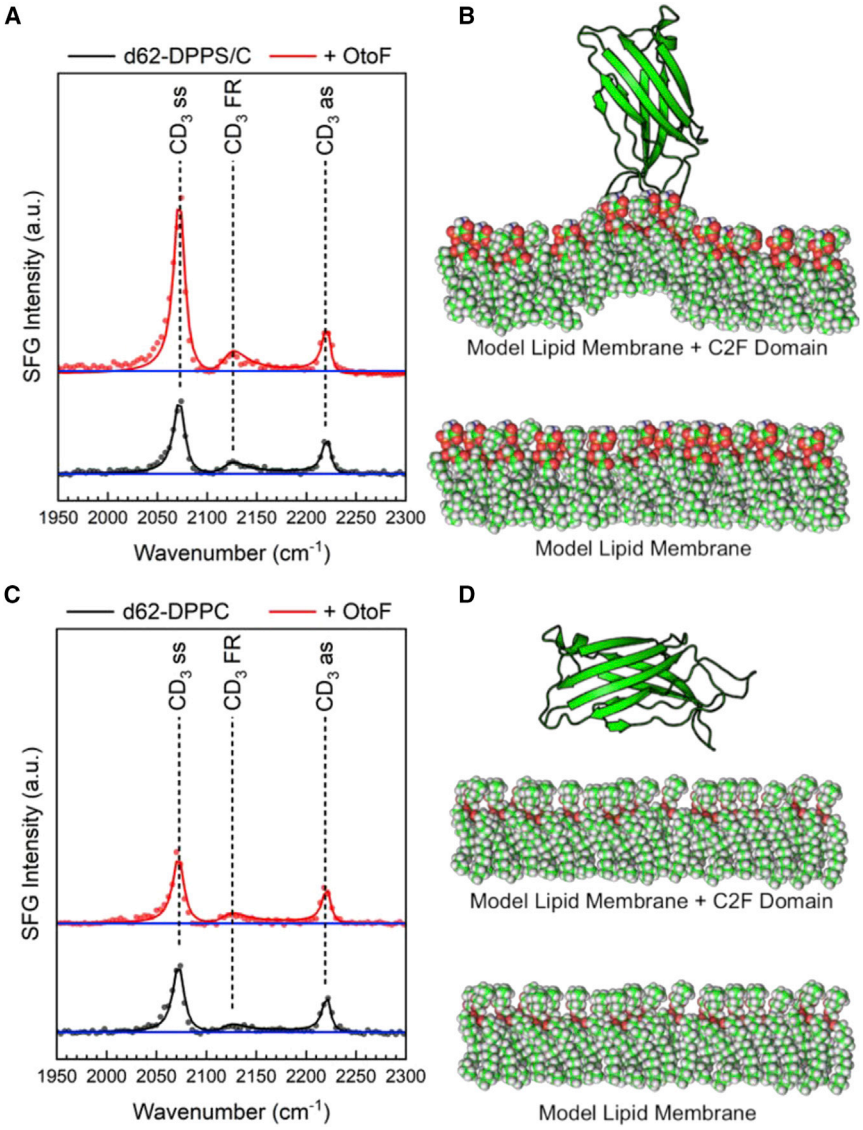

FIGURE 2 Depicts CD region *ssp* polarization combination SFG spectrum of (*A*) the 1:1 molar ratio d62-DPPS and d62-DPPC lipid monolayer before (*black*) and after (*red*) otoferlin C2F domain is injected into the subphase, and (*B*) a cartoon schematic of the otoferlin C2F domain interacting with the lipid monolayer is shown. The schematic depicts the lipid dimpling after the C2F domain of otoferlin adsorbs to the lipid monolayer. The pure d62-DPPC lipid monolayer (*C*) before (*black*) and after (*red*) otoferlin C2F domain is injected into the subphase, and (*D*) a cartoon schematic of the otoferlin C2F domain interacting with the lipid monolayer is shown. Spectra are offset for clarity, and the blue line represents the baseline. To see this figure in color, go online.

be noted that previous studies have reported that high salt concentrations can affect lipid SFG spectra because of $\chi(3)$ contributions based on electrostatic fields across monolayers (55). A recent study by the Geiger group shows that at mM salt concentrations, water OH signals can be affected by $\chi(3)$ effects, whereas the CH resonances are unaffected (56). The CD modes here are spectrally separated from any water modes, and no effect is expected.

For the case of adsorption to the 1:1 ratio, dDPPS/dDPPC lipid monolayer amplitudes corresponding to CD_3 groups increased, whereas comparatively, the amplitudes of the CD_2 groups do not noticeably change (Fig. 2 *A*). No amplitude change was observed for protein adsorption to the pure dDPPC lipid monolayer, consistent with previous results showing that C2F domain of otoferlin does not bind to zwitterionic lipids (Fig. 2 *C*; (4,11,29)). Typically, the ratio of the methyl and methylene symmetric stretches before and after protein interaction can quantify lipid order (14,48). Interestingly, we do not observe a discernable difference in the amplitude of the CD_2 symmetric stretch, making the conventional method of determining lipid ordering difficult. What we measure instead is the lipid orientation change. One method that we can use to quantify lipid orientation is to take the ratio of the CD_3 symmetric stretch vibration near 2075 cm^{-1} and CD_3 asymmetric stretch vibration near 2225 cm^{-1} (24,32). Thus, when comparing final orientation ratios, a value that increases after protein adsorption suggests that the acyl chains of the lipids are orientating with an increasing tilt angle away from the surface normal (24,32). For the C2F domain interacting with a dDPPS/dDPPC lipid monolayer, the ratio of the CD_3 symmetric and CD_3 asymmetric vibrations increases from 1.38 $\pm$ 0.07 to 1.61 $\pm$ 0.08, a 17% increase. There was a statistically significant difference between groups as determined

Please cite this article in press as: Golbek et al., Otoferlin C2F Domain-Induced Changes in Membrane Structure Observed by Sum Frequency Generation, Biophysical Journal (2019), https://doi.org/10.1016/j.bpj.2019.09.010

TABLE 1 CD Region *ssp* Polarization SFG Fitting Results of Otoferlin C2F Domain Interacting with dDPPS/dDPPC and dDPPC Lipid Monolayers

Experiment	$\chi_{NR}^{(2)}$	φ_{NR}	ω_n (cm^{-1})	Γ_n (cm^{-1})	A_n
dDPPS/dDPPC	0	6.27	2072	13.35	−0.0484
			2122	28.66	−0.0349
			2221	9.81	0.0253
dDPPS/dDPPC	0	6.27	2072	13.35	−0.0752
			2122	28.66	−0.0480
			2221	9.81	0.0289
dDPPC	0	6.27	2072	13.35	−0.0464
			2122	28.66	−0.0271
			2221	9.81	0.0252
dDPPC + OtoF	0	6.27	2072	13.35	−0.0459
			2122	28.66	−0.0326
			2221	9.81	0.0252

by a one-way analysis of variance ($F(1,6) = 5.987$, $p = 0.0002$). Conversely, for the dDPPC lipid monolayer after protein adsorption, the orientation ratio stays constant at 1.4, a 0% change (Fig. 2 *C*), suggesting that the C2F domain does not affect the membrane orientation or structure (Fig. 2 *D*). The measured orientation ratio change only for the dDPPS/dDPPC lipid monolayer suggest that the C2F domain, after adsorption, dimples the membrane, causing a lipid orientation change. The values of 1.38 ± 0.07 and 1.61 ± 0.08 result in chain tilt angles of 17.6 and 19.4° to the surface normal, respectively (further explanation of the calculations can be found in the Supporting Materials and Methods). The dimpling caused by the insertion and subsequent interaction of the otoferlin C2F domain with the dDPPS/dDPPC lipid monolayer causes the lipids to orientate further away from the surface normal, which is measured by the increased ratio of the CD_3 symmetric and asymmetric stretching vibrations (32). There is only a very small difference between the calculated acyl chain tilt angles, and this is not surprising because scanning transmission electron microscope images of the synaptotagmin-mediated bending of the membrane can be seen to cause the lipids to adopt various angles simultaneously in one image (10). Thus, because our SFG beam at the lipid membrane surface collects an ensemble of orientations at the anisotropic surface, our calculations may only determine a statistically significant difference of ~1° of tilt angle difference when, in fact, the membrane is quite dimpled at various locations across the membrane. Lipid dimpling, measured by lipid orientation change, is important for getting the membrane ready for vesicle fusion, which is suggested to be one of the primary functions of the C2 domains (10,29).

The C2F domain binds to a cell membrane in an upright orientation

To determine the orientation of the C2F domain (Fig. 3 *A*) on a 1:1 phosphoserine and phosphocholine mixed lipid bilayer, we recorded SFG spectra from the C2F domain in situ in phosphate-buffered saline buffer and in the presence of calcium. A schematic of the sample cell is depicted in Fig. 3 *C*. In implementing this approach, a model lipid membrane was prepared by depositing lipid vesicles at a CaF_2 prism interface and probing the lipid bilayer-protein-buffer interface through the backside of a CaF_2 equilateral prism. Experimental SFG amide-I spectra collected in *p*-polarized SFG, *p*-polarized VIS, *p*-polarized IR (*ppp*) and *ssp* are shown in Fig. 4 *A*, and *spp* is shown in the Fig. S3. The *ppp* and *ssp* spectra are dominated by features near 1630 cm^{-1} (a peak) and 1670 cm^{-1} (a dip). These resonances are commonly assigned to β-sandwich secondary structures, and this structure motif is present in the native otoferlin C2F domain (Fig. 3 *A*; (16)).

Protein SFG spectra are heavily influenced by interference between signals from different secondary-structure elements and protein side chains, based on their relative orientation and energy. SFG has previously been used to study lipid monolayers at the air/water interface (15,32,49–52,57,58), model lipid bilayers (59–62), and small proteins and peptides interaction with each type of model membrane (14–16,53,59,61–70). For small proteins and peptides, the direct analysis of SFG amide-I spectra

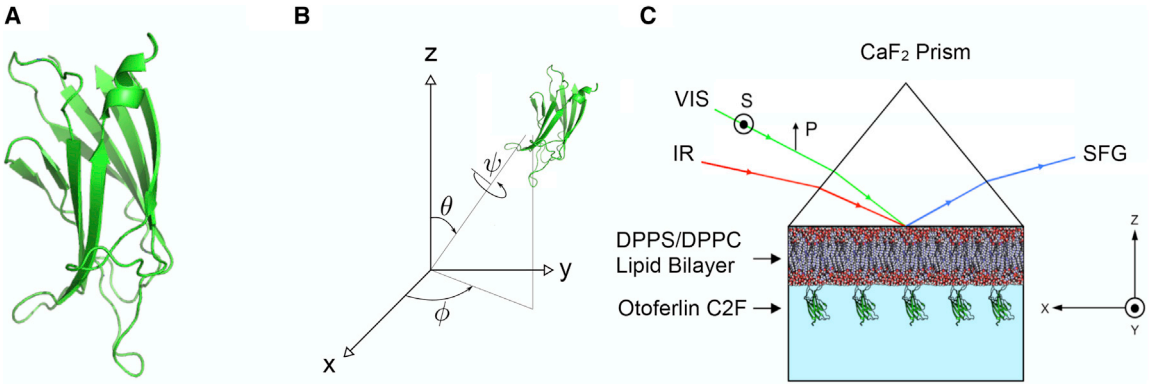

FIGURE 3 Structure of the otoferlin C2F domain from PDB 4IQH (*A*). Shown are the coordinate system and Euler angles of the protein orientation in the laboratory frame (*B*). Shown is the experimental setup for in situ SFG measurements of OtoF-bilayer binding (*C*). To see this figure in color, go online.

Please cite this article in press as: Golbek et al., Otoferlin C2F Domain-Induced Changes in Membrane Structure Observed by Sum Frequency Generation, Biophysical Journal (2019), https://doi.org/10.1016/j.bpj.2019.09.010

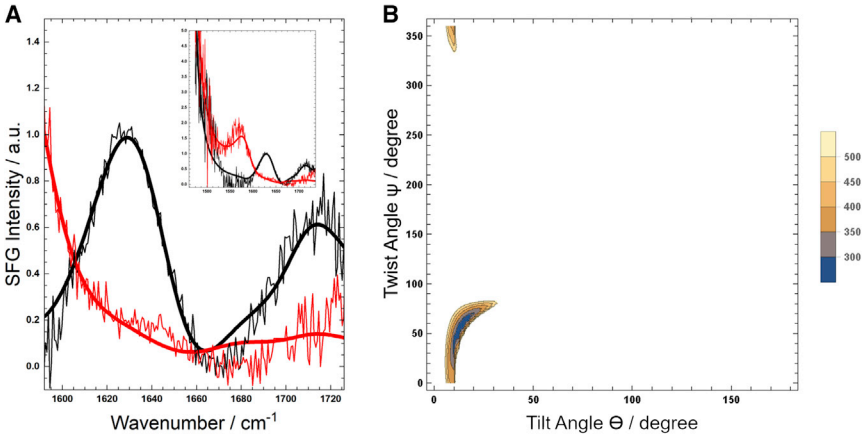

FIGURE 4 (*A*) Optimal fit of the experimental *ppp* (*black*) and *ssp* (*red*) data of OtoF, for a protein tilt angle $\theta = 22 \pm 2°$ and a twist angle $\psi = 74 \pm 2°$. (*B*) Shown is an error-weighted two-dimensional residual sum-of-squares (2D-RSS) plot of the amide-I (1600–1700 cm^{-1}) region composed of ~10,000 spectral calculations at a θ and ψ resolution of 2.5° that indicates that the experimental spectra can only be modeled well for a small range of protein orientations. In the white area, the error-weighted RSS is more than twice the minimal error-weighted RSS value (255). The 2D-RSS plot for the whole modeled spectral range (1440–1740 cm^{-1}) can be found in Fig. S4. To see this figure in color, go online.

by peak fitting vibrational spectra relating to the C=O of the amide backbone can provide information about the orientation and structure (67,71,72). However, because the otoferlin C2F domain structure is complex, which leads to severe spectral interference and convolution, it is not possible to obtain unambiguous information about the protein conformation by direct spectral inspection and fitting. To solve this problem and to make full use of the structural information within the SFG spectra, we have developed a framework for calculating theoretical SFG spectra from PDB (Protein Data Bank) (24,33,42) and molecular dynamics structure files (25,73,74). Thus, spectra for this study were calculated from PDB models. In addition, by calculating spectra for different protein orientations with respect to the surface and matching experimental and calculated spectra for different orientations, one can determine the surface binding geometry.

Because the crystal structure of otoferlin C2F does not exist, we used the otoferlin homolog dysferlin C2A for our SFG calculations (11,75,76). Fig. 4 *A* shows theoretical SFG spectra calculated with a one-exciton amide-I model for the crystal structure of otoferlin C2F domain (PDB 4IQH), for a tilt angle $\theta = 22 \pm 2°$ and a twist angle $\psi = 74 \pm 2°$ (see the Materials and Methods; Supporting Materials and Methods for a detailed description of the calculation methodology), leading to the protein orientation depicted in Fig. 5. Besides the overall intensities and orientations of the protein's side-chain and amide-I modes and of the lipid C=O mode, no adjustable parameters were used to match the calculated spectra to the experimental data. The calculations match the experimental spectral features well for only a small region in the protein's (θ, ψ)-range (see Figs. 3 *B* and 4 *B* for the definition of these angles). In this region, the calculated spectra reproduce the experimentally observed peak near 1630 cm^{-1} (a peak) and the dip 1670 cm^{-1} (a dip). Importantly, the relative intensities of the *ppp* and *ssp* spectra match the experimental data. The agreement of experimental and calculated spectra indicates that otoferlin C2F domain maintains a folded structure close to its native state when docking with a lipid bilayer.

Although the *ssp* and *ppp* (achiral) spectra from 1440 to 1740 cm^{-1} can be reproduced well with the calculations, the intensity of the calculated *spp* (chiral) spectrum (see Fig. S3) is underestimated in comparison to the experimental spectrum. When calculating the *spp* spectrum with the same model and orientation as for the *ssp* and *ppp*

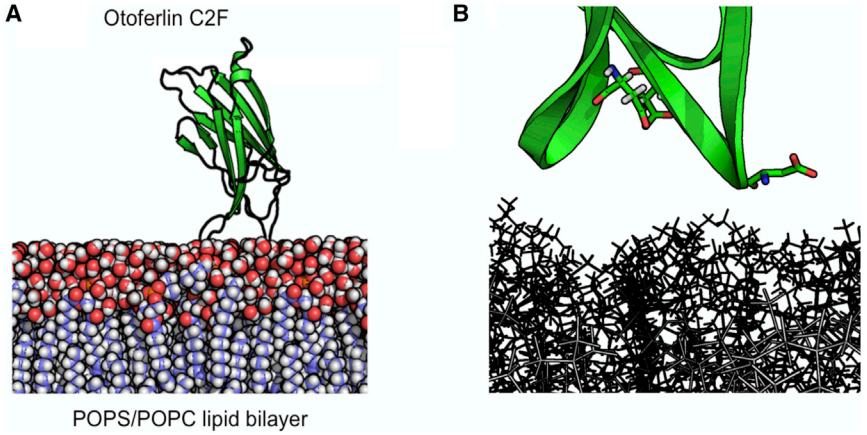

FIGURE 5 Extracted orientation from the raster search. (*A*) Average orientation for OtoF on a lipid bilayer surface from SFG spectra calculations show significant spectral match with experimental spectra. (*B*) Zoomed in view of the otoferlin C2F domain binding loops with the aspartic acids is shown. To see this figure in color, go online.

spectrum, the calculated *spp* spectrum is ~10 times smaller than the experimental spectrum, whereas the relative *ssp* and *ppp* intensities are reproduced well. As shown in Fig. S3, this discrepancy can be explained by the fact that chiral SFG signals are very sensitive to chirality in the macromolecular ordering; for a structure composed of nine monomers that are rotated by 20° (over Euler angle ϕ) with respect to each other, the chiral signal (*spp*) per monomer goes up by a factor of 130, whereas the achiral signals (*ssp* and *ppp*) per monomer goes down by a factor of 2 because of destructive interference. Future work, aided by molecular dynamics simulations, might be able to resolve the structure at the macromolecular level.

The tilt angle obtained with the global *ssp* and *ppp* fit (22° ± 2°) suggests that the C2F domain is docked in an upright orientation relative to the membrane surface with the loops on one side of the domain in contact with the membrane. Because (for an azimuthal isotropy) the homodyne SFG signal for a given set of (θ, ψ)-values equals that of (180 – θ, 180 + ψ), the SFG measurement cannot be used to discriminate between a tilt angle of 22 and 158°. However, previous studies of C2 domains have concluded that these domains have very specific binding loops with conserved aspartic acid residues, whereby they form a calcium bridge with the cell membrane (8). Applying these constraints to our homodyne SFG signal, we can exclude 158° and conclude that the protein must be at a tilt angle of 22°. This observation is further supported in which our lipid binding geometry is similar to previous simulations that report synaptotagmin 1's C2A domain also orients at the membrane interface at a tilt angle of 37.1 ± 9.5°, with the binding loops in contact with the membrane (77). However, the tilt angles of the C2 domains of synaptotagmin have also been proposed to adopt other angles in an apparently calcium-sensitive manner (78).

To further place the importance of the orientation in context, previous studies on the C2 domains of synaptotagmin 1 have concluded that the C2B domain of the protein adopts two distinct angles relative to the bilayer and that the change in orientation is calcium sensitive and necessary for synaptotagmin activity. Specifically, in the absence of calcium, the C2B domain lies nearly parallel to the bilayer in a membrane fusion incompetent state. Elevated calcium concentrations result in coordination of calcium ions by the negatively charged loops of the C2B domain, which negates the electrostatic repulsion between the loops and the lipid bilayer, resulting in reorientation of the domain such that the loops insert into the membrane (79,80). In the case of synaptogamin, this reorientation and insertion are thought to be critical for synchronous release of neurotransmitter. A greater variation in orientation has been reported for the C2 domains of synaptotagmin 7 (81), a protein that also differs in the insertion depth of the loops of the C2 domains and in the speed of exocytosis. Although there are considerable differences in domain orientation and, hence, insertion depth, no information is available for any domain of the ferlin family of proteins. In addition, most studies have used cysteine mutagenesis and probe conjugation in the loops of the C2 domain, which in principle could lead to artifacts related to the labels. Our method circumvents the need for invasive labeling, and analysis of our results suggest that in the presence of calcium, the C2F domain of otoferlin may adopt a steep angle not unlike the C2B domain of synaptotagmin 1 in calcium. Because the C2F domain does not apparently lie parallel to the surface but rather orients nearly perpendicular, C2F may contribute to membrane fusion like the C2B domain of synaptotagmin. Indeed, recent truncation studies have concluded that the C2F domain is critical for rescuing exocytosis in sensory hair cells, consistent with a function in membrane fusion (3,82). Furthermore, the binding loops play an important role in the docking of the C2F domain, and thus, the types of residues in the binding loops need to be considered. Using our combined simulation and experimental approach, we can further identify which specific loops within otoferlin's C2F domain directly interact with the lipid membrane. The two specific loops within the C2F domain that directly interact with the lipids are highlighted in Fig. 5 *B*. These loops contain hydrophobic, positively charged, and negatively charged residues. Previous studies have demonstrated that the hydrophobic and hydrophilic residues in the binding loops have a large impact on the docking kinetics of the C2 domains (78). This orientation also places the aspartic acid residues near the membrane surface, which is important because of the calcium bridge that forms between the aspartic acid residue and the phosphoserine headgroup of the lipids before the protein docks with the membrane surface (4,6,83).

CONCLUSIONS

This study highlights a methodology to directly probe the orientation of the C2F domain of otoferlin. The results suggest that the C2F domain dimples the membrane with an upright docking angle to the membrane surface, leading to the identification of binding loops positioned toward the lipid membrane surface. Additionally, this experimental protocol can be applied to other C2 domains in the ferlin family and ultimately directly monitor the interaction of a ferlin's C2 domain. Moving forward from this initial investigation, we can use this study as the basis to perform a series of detailed studies to investigate the impact of mutations in the C2 domains of ferlins and the impact on membrane dimpling and protein orientation.

SUPPORTING MATERIAL

Supporting Material can be found online at https://doi.org/10.1016/j.bpj.2019.09.010.

AUTHOR CONTRIBUTIONS

J.E.B., T.W.G., M.P., S.J.R., C.P.J., and T.W. designed the experiments. J.E.B., T.W.G., M.P, C.P.J., and T.W. conducted the SFG experiments. S.J.R. and T.W. conducted SFG spectral calculations. The manuscript was written by all co-authors.

ACKNOWLEDGMENTS

This work was supported by the John C. Erkkila, M. D. Endowment for Health and Human Performance, National Institute of Deafness and Other Communication Disorders grant R01DC014588 to C.P.J. and the National Science Foundation award 1905091.

REFERENCES

1. Baio, J. E., A. Zane, …, T. Weidner. 2014. Diatom mimics: directing the formation of biosilica nanoparticles by controlled folding of lysine-leucine peptides. *J. Am. Chem. Soc.* 136:15134–15137.
2. Roux, I., S. Safieddine, …, C. Petit. 2006. Otoferlin, defective in a human deafness form, is essential for exocytosis at the auditory ribbon synapse. *Cell.* 127:277–289.
3. Chatterjee, P., M. Padmanarayana, …, C. P. Johnson. 2015. Otoferlin deficiency in zebrafish results in defects in balance and hearing: rescue of the balance and hearing phenotype with full-length and truncated forms of mouse otoferlin. *Mol. Cell. Biol.* 35:1043–1054.
4. Johnson, C. P., and E. R. Chapman. 2010. Otoferlin is a calcium sensor that directly regulates SNARE-mediated membrane fusion. *J. Cell Biol.* 191:187–197.
5. Hams, N., M. Padmanarayana, …, C. P. Johnson. 2017. Otoferlin is a multivalent calcium-sensitive scaffold linking SNAREs and calcium channels. *Proc. Natl. Acad Sci. USA.* 114:8023–8028.
6. Pangršič, T., E. Reisinger, and T. Moser. 2012. Otoferlin: a multi-C2 domain protein essential for hearing. *Trends Neurosci.* 35:671–680.
7. Fioravante, D., Y. Chu, …, W. G. Regehr. 2014. Protein kinase C is a calcium sensor for presynaptic short-term plasticity. *eLife.* 3:e03011.
8. Cho, W., and R. V. Stahelin. 2006. Membrane binding and subcellular targeting of C2 domains. *Biochim. Biophys. Acta.* 1761:838–849.
9. Hui, E., J. Bai, and E. R. Chapman. 2006. Ca2+-triggered simultaneous membrane penetration of the tandem C2-domains of synaptotagmin I. *Biophys. J.* 91:1767–1777.
10. Hui, E., C. P. Johnson, …, E. R. Chapman. 2009. Synaptotagmin-mediated bending of the target membrane is a critical step in Ca(2+)-regulated fusion. *Cell.* 138:709–721.
11. Padmanarayana, M., N. Hams, …, C. P. Johnson. 2014. Characterization of the lipid binding properties of Otoferlin reveals specific interactions between PI(4,5)P2 and the C2C and C2F domains. *Biochemistry.* 53:5023–5033.
12. Martorana, A., G. Bellapadrona, …, D. Goldfarb. 2014. Probing protein conformation in cells by EPR distance measurements using Gd3+ spin labeling. *J. Am. Chem. Soc.* 136:13458–13465.
13. Hoffman, I. D. 2012. Protein crystallization for structure-based drug design. *Methods Mol. Biol.* 841:67–91.
14. Golbek, T. W., J. Franz, …, J. E. Baio. 2017. Identifying the selectivity of antimicrobial peptides to cell membranes by sum frequency generation spectroscopy. *Biointerphases.* 12:02D406.
15. Schach, D. K., W. Rock, …, T. Weidner. 2015. Reversible activation of a cell-penetrating peptide in a membrane environment. *J. Am. Chem. Soc.* 137:12199–12202.
16. Ye, S., K. T. Nguyen, …, Z. Chen. 2009. In situ molecular level studies on membrane related peptides and proteins in real time using sum frequency generation vibrational spectroscopy. *J. Struct. Biol.* 168: 61–77.
17. Wu, F. G., P. Yang, …, Z. Chen. 2014. Investigation of drug–model cell membrane interactions using sum frequency generation vibrational spectroscopy: a case study of chlorpromazine. *J. Phys. Chem. C.* 118:17538–17548.
18. Shen, Y.-R. 1984. The Principles of Nonlinear Optics. Wiley-Interscience, New York, p. 575.
19. Ahn, D., and A. Dhinojwala. 2012. Sum frequency generation vibrational spectroscopy of silicone surfaces & interfaces. *In* Silicone Surface Science. M. J. Owen and P. R. Dvornic, eds. Springer, pp. 23–58.
20. Zhuang, X., P. B. Miranda, …, Y. R. Shen. 1999. Mapping molecular orientation and conformation at interfaces by surface nonlinear optics. *Phys. Rev. B.* 59:12632–12640.
21. Wang, H.-F., W. Gan, …, B.-H. Wu. 2005. Quantitative spectral and orientational analysis in surface sum frequency generation vibrational spectroscopy (SFG-VS). *Int. Rev. Phys. Chem.* 24:191–256.
22. Chen, X., J. Wang, …, Z. Chen. 2005. Probing α-helical and β-sheet structures of peptides at solid/liquid interfaces with SFG. *Langmuir.* 21:2662–2664.
23. Wang, J., X. Chen, …, Z. Chen. 2005. Detection of chiral sum frequency generation vibrational spectra of proteins and peptides at interfaces in situ. *Proc. Natl. Acad. Sci. USA.* 102:4978–4983.
24. Hennig, R., J. Heidrich, …, D. Schneider. 2015. IM30 triggers membrane fusion in cyanobacteria and chloroplasts. *Nat. Commun.* 6:7018.
25. Schmüser, L., S. Roeters, …, T. Weidner. 2017. Determination of absolute orientation of protein α-helices at interfaces using phase-resolved sum frequency generation spectroscopy. *J. Phys. Chem. Lett.* 8:3101–3105.
26. Lutz, H., V. Jaeger, …, T. Weidner. 2015. Biomimetic growth of ultrathin silica sheets using artificial amphiphilic peptides. *Adv. Mater. Interfaces.* 2:1500282.
27. Donovan, M. A., Y. Y. Yimer, …, T. Weidner. 2016. Ultrafast reorientational dynamics of leucine at the air-water interface. *J. Am. Chem. Soc.* 138:5226–5229.
28. Pandey, R., K. Usui, …, T. Weidner. 2016. Ice-nucleating bacteria control the order and dynamics of interfacial water. *Sci. Adv.* 2:e1501630.
29. Marty, N. J., C. L. Holman, …, C. P. Johnson. 2013. The C2 domains of otoferlin, dysferlin, and myoferlin alter the packing of lipid bilayers. *Biochemistry.* 52:5585–5592.
30. Cho, N.-J., C. W. Frank, …, F. Höök. 2010. Quartz crystal microbalance with dissipation monitoring of supported lipid bilayers on various substrates. *Nat. Protoc.* 5:1096–1106.
31. Hardy, G. J., R. Nayak, and S. Zauscher. 2013. Model cell membranes: techniques to form complex biomimetic supported lipid bilayers via vesicle fusion. *Curr. Opin. Colloid Interface Sci.* 18:448–458.
32. Ma, G., and H. C. Allen. 2006. DPPC Langmuir monolayer at the air-water interface: probing the tail and head groups by vibrational sum frequency generation spectroscopy. *Langmuir.* 22:5341–5349.
33. Roeters, S. J., C. N. van Dijk, …, S. Woutersen. 2013. Determining in situ protein conformation and orientation from the amide-I sum-frequency generation spectrum: theory and experiment. *J. Phys. Chem. A.* 117:6311–6322.
34. Gorbunov, R. D., D. S. Kosov, and G. Stock. 2005. Ab initio-based exciton model of amide I vibrations in peptides: definition, conformational dependence, and transferability. *J. Chem. Phys.* 122:224904.
35. Hamm, P., and M. Zanni. 2011. Concepts and Methods of 2D Infrared Spectroscopy. Cambridge University Press, Cambridge, UK.
36. Krimm, S., and J. Bandekar. 1986. Vibrational spectroscopy and conformation of peptides, polypeptides, and proteins. *Adv. Protein Chem.* 38:181–364.
37. Barth, A. 2007. Infrared spectroscopy of proteins. *Biochim. Biophys. Acta.* 1767:1073–1101.
38. Sultanova, N., S. Kasarova, and I. D. Nikolov. 2009. Dispersion properties of optical polymers. *Acta Phys. Pol. A.* 116:585–587.
39. Hand, D. B. 1935. The refractivity of protein solutions. *J. Biol. Chem.* 108:703–707.

40. Bucciarelli, A., V. Mulloni, …, A. Quaranta. 2018. A comparative study of the refractive index of silk protein thin films towards biomaterial based optical devices. *Opt. Mater.* 78:407–414.

41. Hale, G. M., and M. R. Querry. 1973. Optical constants of water in the 200-nm to 200-μm wavelength region. *Appl. Opt.* 12:555–563.

42. Verreault, D., S. Alamdari, …, T. Weidner. 2018. Ice-binding site of surface-bound type III antifreeze protein partially decoupled from water. *Phys. Chem. Chem. Phys.* 20:26926–26933.

43. Roeters, S. J., E. H. Tronic, …, T. Weidner. 2018. Structure of von Willebrand factor A1 on polystyrene determined from experimental and calculated sum frequency generation spectra. *Biointerphases.* 13:06E411.

44. Ohno, P. E., H. F. Wang, and F. M. Geiger. 2017. Second-order spectral lineshapes from charged interfaces. *Nat. Commun.* 8:1032.

45. Bain, C. D. 1995. Sum-frequency vibrational spectroscopy of the solid/liquid interface. *J. Chem. Soc., Faraday Trans.* 91:1281–1296.

46. Moore, F. G., K. A. Becraft, and G. L. Richmond. 2002. Challenges in interpreting vibrational sum frequency spectra: deconvoluting spectral features as demonstrated in the calcium fluoride—water—sodium dodecylsulfate system. *Appl. Spectrosc.* 56:1575–1578.

47. Brockman, H. 1999. Lipid monolayers: why use half a membrane to characterize protein-membrane interactions? *Curr. Opin. Struct. Biol.* 9:438–443.

48. Franz, J., T. Bereau, …, D. Schneider. 2017. Nitrated fatty acids modulate the physical properties of model membranes and the structure of transmembrane proteins. *Chemistry.* 23:9690–9697.

49. Liljeblad, J. F., V. Bulone, …, C. M. Johnson. 2010. Phospholipid monolayers probed by vibrational sum frequency spectroscopy: instability of unsaturated phospholipids. *Biophys. J.* 98:L50–L52.

50. Maget-Dana, R. 1999. The monolayer technique: a potent tool for studying the interfacial properties of antimicrobial and membrane-lytic peptides and their interactions with lipid membranes. *Biochim. Biophys. Acta.* 1462:109–140.

51. Mauri, S., R. Pandey, …, T. Weidner. 2015. Bovine and human insulin adsorption at lipid monolayers: a comparison. *Front. Phys.* 3:51.

52. Watry, M. R., T. L. Tarbuck, and G. L. Richmond. 2003. Vibrational sum-frequency studies of a series of phospholipid monolayers and the associated water structure at the vapor/water interface. *J. Phys. Chem. B.* 107:512–518.

53. Rzeźnicka, I. I., R. Pandey, …, T. Weidner. 2014. Formation of lysozyme oligomers at model cell membranes monitored with sum frequency generation spectroscopy. *Langmuir.* 30:7736–7744.

54. Franz, J., M. J. van Zadel, and T. Weidner. 2017. A trough for improved SFG spectroscopy of lipid monolayers. *Rev. Sci. Instrum.* 88:053106.

55. Casper, C. B., D. Verreault, …, H. C. Allen. 2016. Surface potential of DPPC monolayers on concentrated aqueous salt solutions. *J. Phys. Chem. B.* 120:2043–2052.

56. Doğangün, M., P. E. Ohno, …, F. M. Geiger. 2018. Hydrogen-bond networks near supported lipid bilayers from vibrational sum frequency generation experiments and atomistic simulations. *J. Phys. Chem. B.* 122:4870–4879.

57. Liljeblad, J. F. D., V. Bulone, …, C. M. Johnson. 2011. Supported phospholipid monolayers. The molecular structure investigated by vibrational sum frequency spectroscopy. *J. Phys. Chem. C.* 115:10617–10629.

58. Franz, J., M. Lelle, …, T. Weidner. 2016. SAP(E) – a cell-penetrating polyproline helix at lipid interfaces. *Biochim. Biophys. Acta.* 1858:2028–2034.

59. Chen, X., J. Wang, …, Z. Chen. 2007. Multiple orientation of melittin inside a single lipid bilayer determined by combined vibrational spectroscopic studies. *J. Am. Chem. Soc.* 129:1420–1427.

60. Wang, T., D. Li, …, Z. Chen. 2011. Single lipid bilayers constructed on polymer cushion studied by sum frequency generation vibrational spectroscopy. *J Phys Chem C Nanomater Interfaces.* 115:7613–7620.

61. Chen, X., and Z. Chen. 2006. SFG studies on interactions between antimicrobial peptides and supported lipid bilayers. *Biochim. Biophys. Acta.* 1758:1257–1273.

62. Chen, X., J. Wang, …, Z. Chen. 2007. Real-time structural investigation of a lipid bilayer during its interaction with melittin using sum frequency generation vibrational spectroscopy. *Biophys. J.* 93:866–875.

63. Ding, B., and Z. Chen. 2012. Molecular interactions between cell penetrating peptide Pep-1 and model cell membranes. *J. Phys. Chem. B.* 116:2545–2552.

64. Liu, Y., J. Jasensky, and Z. Chen. 2012. Molecular interactions of proteins and peptides at interfaces studied by sum frequency generation vibrational spectroscopy. *Langmuir.* 28:2113–2121.

65. Nguyen, K. T., R. Soong, …, Z. Chen. 2010. Probing the spontaneous membrane insertion of a tail-anchored membrane protein by sum frequency generation spectroscopy. *J. Am. Chem. Soc.* 132:15112–15115.

66. Nguyen, K. T., S. V. Le Clair, …, Z. Chen. 2009. Molecular interactions between magainin 2 and model membranes in situ. *J. Phys. Chem. B.* 113:12358–12363.

67. Nguyen, K. T., J. T. King, and Z. Chen. 2010. Orientation determination of interfacial β-sheet structures in situ. *J. Phys. Chem. B.* 114:8291–8300.

68. Thennarasu, S., R. Huang, …, A. Ramamoorthy. 2010. Limiting an antimicrobial peptide to the lipid-water interface enhances its bacterial membrane selectivity: a case study of MSI-367. *Biochemistry.* 49:10595–10605.

69. Wang, J., S. M. Buck, and Z. Chen. 2002. Sum frequency generation vibrational spectroscopy studies on protein adsorption. *J. Phys. Chem. B.* 106:11666–11672.

70. Yang, P., A. Ramamoorthy, and Z. Chen. 2011. Membrane orientation of MSI-78 measured by sum frequency generation vibrational spectroscopy. *Langmuir.* 27:7760–7767.

71. Nguyen, K. T., S. V. Le Clair, …, Z. Chen. 2009. Orientation determination of protein helical secondary structures using linear and nonlinear vibrational spectroscopy. *J. Phys. Chem. B.* 113:12169–12180.

72. Liu, Y., J. Tan, …, S. Ye. 2018. Influenza A M2 transmembrane domain tunes its conformational heterogeneity and structural plasticity in the lipid bilayer by forming loop structures. *Chem. Commun. (Camb.).* 54:5903–5906.

73. Schach, D., C. Globisch, …, T. Weidner. 2014. Sticky water surfaces: helix–coil transitions suppressed in a cell-penetrating peptide at the air-water interface. *J. Chem. Phys.* 141:22D517.

74. Lu, H., H. Lutz, …, T. Weidner. 2018. Calcium-induced molecular rearrangement of peptide folds enables biomineralization of vaterite calcium carbonate. *J. Am. Chem. Soc.* 140:2793–2796.

75. Abdullah, N., M. Padmanarayana, …, C. P. Johnson. 2014. Quantitation of the calcium and membrane binding properties of the C2 domains of dysferlin. *Biophys. J.* 106:382–389.

76. Fuson, K., A. Rice, …, R. B. Sutton. 2014. Alternate splicing of dysferlin C2A confers Ca2+-dependent and Ca2+-independent binding for membrane repair. *Structure.* 22:104–115.

77. Osterberg, J. R., N. L. Chon, …, J. D. Knight. 2015. Membrane docking of the synaptotagmin 7 C2A domain: electron paramagnetic resonance measurements show contributions from two membrane binding loops. *Biochemistry.* 54:5684–5695.

78. Vermaas, J. V., and E. Tajkhorshid. 2017. Differential membrane binding mechanics of synaptotagmin isoforms observed in atomic detail. *Biochemistry.* 56:281–293.

79. Bai, J., W. C. Tucker, and E. R. Chapman. 2004. PIP2 increases the speed of response of synaptotagmin and steers its membrane-penetration activity toward the plasma membrane. *Nat. Struct. Mol. Biol.* 11:36–44.

80. Bai, J., C. T. Wang, …, E. R. Chapman. 2004. Fusion pore dynamics are regulated by synaptotagmin*t-SNARE interactions. *Neuron.* 41:929–942.

81. Chon, N. L., J. R. Osterberg, …, H. Lin. 2015. Membrane docking of the synaptotagmin 7 C2A domain: computation reveals interplay between electrostatic and hydrophobic contributions. *Biochemistry.* 54:5696–5711.

82. Tertrais, M., Y. Bouleau, …, D. Dulon. 2019. Viral transfer of mini-otoferlins partially restores the fast component of exocytosis and uncovers ultrafast endocytosis in auditory hair cells of otoferlin knock-out mice. *J. Neurosci.* 39:3394–3411.

83. Ramakrishnan, N. A., M. J. Drescher, …, D. G. Drescher. 2014. Calcium regulates molecular interactions of otoferlin with soluble NSF attachment protein receptor (SNARE) proteins required for hair cell exocytosis. *J. Biol Chem.* 289:8750–8766.